Supporting Information

Isolated Cobalt-Nitrogen Sites on High-Curvature Carbon Achieving Industrial-Level Current Density and pH-Universal CO_2 Electroreduction

Jun Wang, [†] *Xifan Chen,* [†] *Zhengkun Yang,* [†] *Juan-Ding Xiao,* [†] *Chenchen Qin,* [†] *Zhenhua Yan,* [‡] *Zhiyuan Wang,* [Δ] *Jia Yang,* [†,] * *Junzhong Wang*[†,*]

[†] Institutes of Physical Science and Information Technology, Anhui Graphene Materials Research Center, Anhui University, Hefei, Anhui 230601, China

[‡] Key Laboratory of Advanced Energy Materials Chemistry (Ministry of Education), Nankai University, Tianjin 300071, China

[Δ] Henan Institute of Advanced Technology, Zhengzhou University, Zhengzhou 450001, China

* E-mail: yj4368@ahu.edu.cn, wangjz@ahu.edu.cn

1. Materials and Methods

Synthesis of cobalt-1,10-phenanthroline complex: 4.5 mg Cobalt(II) acetate was dissolved in 1 mL ethanol, 10 mg 1,10-phenanthroline monohydrate was dissolved in 1 mL ethanol. Then the phenanthroline solution was added slowly with constant stirring to cobalt(II) acetate solution and stirred for 1 hours to get cobalt-1,10-phenanthroline complex solution.

Synthesis of c-Co SAC: Nanodiamond was refluxed in mixture of H_2SO_4 and HNO_3 (3:1) at 150 ℃ for 24 hours then washed with water throughly and freeze-dried. The obtained nanodiamond was then thermally treated at 1500 ℃ for 2 hours under Ar to get onion-like carbon. For the synthesis of c-Co SAC, 30 mg onion-like carbon was dispersed in 2 mL ethanol, then mixed with 320 uL cobalt-1,10-phenanthroline complex solution under sonication. Then it was heated at 60 ℃ under stirring for 5 hours. After being vaccum dried, the obtained powder was thermally treated at 700 ℃ under Ar for 2 hours to yield c-Co SAC.

Synthesis of p-Co SAC: Graphene was prepared according to our previous report (J. Am. Chem. Soc. 2011, 133, 8888). The synthesis process of p-Co SAC were the same with c-Co SAC except that onion-like carbon was replaced by graphene.

Characterizations: Aberration-corrected high angle annular dark-field scanning transmission electron microscopy (AC HAADF-STEM) was conducted on Titan Themis Z atomic resolution analytical microscope operating at an accelerating voltage of 300 kV. High-resolution transmission electron microscopy (HRTEM) was conducted on JEM-F200 operating at an accelerating voltage of 200 kV. Powder X-ray diffraction (PXRD) patterns were obtained using a Rigaku Miniflex600 X-ray powder diffractometer equipped with a Cu-Kα radiation source (λ=0.154 nm). X-ray photoelectron spectroscopy (XPS) measurements were performed on X-ray photoelectron spectrometer (ESCALAB 250Xi). Raman spectra were recorded on a raman spectroscopy (Via-Reflex). X-ray absorption fine spectroscopy (XAFS) measurements were carried out at BL1W1B station in the Beijing Synchrotron Radiation Facility (BSRF) in a fluorescence mode. The storage ring was working at the energy of 2.5 GeV with an average electron current of 250 mA. All samples were pelletized as disks of 10 mm diameter using PVDF as binder. The acquired EXAFS data were processed according to the standard procedures using the ATHENA module implemented in the IFEFFIT software packages. The EXAFS spectra were obtained by subtracting the post-edge background from the overall absorption and then normalizing with respect to the edge-jump step.

CO_2 reduction on H-cell: Electrochemical measurements were carried out in a three-electrode system on a CHI760E electrochemical workstation at room temperature. Carbon paper loaded with catalysts served as working electrode, Ag/AgCl (3.5M KCl) served as reference electrode and graphite rod served as counter electrode. A cation exchange membrane (nafion 117) was used to seperate the anode part and cathode part. 2 mg catalyst was mixed with 1 mL ethanol and 10 μL Nafion solution followed by sonication to form a homogeneous ink, which was then drop casted onto the carbon paper. The mass loading of the catalyst was 0.5 mg/cm^2. The electrolyte (0.5M $KHCO_3$) was saturated with CO_2 prior to CO_2 reduction experiments. During CO_2 reduction, CO_2 was continuously

bubbled into cathode part with flow rate of 20 mL/min. LSV curves were collected with scan rate of 10 mV/s. The gas products were analyzed by on-line gas chromatography (Agilent 8890). H_2 was detected using a TCD detector. CO was converted to CH_4 by a methanation reactor and then analyzed by FID detector. The Faradaic efficiency of the gas products was calculated as follows:

$$FE = \frac{v \times n \times F}{J} \times 100\%$$

where v is the production rate of CO or H_2, n is the electron transfer number, which is 2 for CO and H_2, F is Faradaic constant, which is 96485 C/mol, J is current density.

TOF was calculated as follows:

$$TOF = \frac{J_{product}/nF}{m \times \omega/M_{metal}} \times 3600$$

where $J_{product}$ is the partial current for CO, m is the mass of catalyst on the electrode, ω represents the metal loading in the catalyst, M_{metal} is the atomic mass of Co.

CO_2 reduction on flow-cell： Flow cell measurements were performed in a flow cell reactor. The catalyst was spray coated onto gas diffusion layer (Sigracet 29BC), which served as working electrode. Ag/AgCl (3.5M KCl) served as reference electrode and nickel foam served as counter electrode. The anode part and cathode part were seperated by an anion exchange membrane. During the measurements, CO_2 passed through the gas chamber with a flow rate of 30 mL/min. The electrolyte was circulated by a peristaltic pump at a rate of 10 mL/min.

In-situ attenuated total reflection-infrared spectroscopy (ATR-IR): ATR-IR was carried out on a Thermoscientific iS50 FT-IR spectrometer equipped with an MCT detector cooled with liquid nitrogen. Experiments were conducted on H-type cell. The Au-coated Si semi-cylindrical prism (20 mm in diameter) was employed as the working electrode and the IR refection element. The catalyst was drop casted onto the working electrode with loading of 0.5 mg/cm^2. Ag/AgCl (3.5M KCl) served as reference electrode and graphite rod served as counter electrode. A cation exchange membrane (nafion 117) was used to seperate the anode part and cathode part.

DFT calculations: All the spin-polarized DFT calculations on this system were conducted by Vienna ab initio simulation package.[1] The projector-augmented wave (PAW) method and Perdew-Burke-Ernzerhof (PBE)[2,3] functional within the generalized gradient approximation (GGA) were applied to describe ionic cores and exchange-correlation effects, respectively. A cutoff energy of 500 eV was adopted and the Grimme method for DFT-D3 was used to account for van der Waals (vdW) interactions.[3] The convergence criteria for residual force and energy were set to 0.02 eV/Å and 10−5 eV, respectively. The Brillouin zone for was sampled with 2 × 2 × 1 Gamma centered special k points

grid for geometry optimization, respectively.

(1) Kresse, G. *et al.* Efficient iterative schemes for ab initio total-energy calculations using a plane-wave basis set. *Phys. Rev. B* **54**, 11169 (1996).
(2) Perdew, J. P. *et al.* Generalized gradient approximation made simple. *Phys. Rev. Lett.* **77**, 3865 (1996).
(3) Grimme, S. Semiempirical GGA-type density functional constructed with a long-range dispersion correction. *J. Comput. Chem*. **27**, 1787 (2006).

2. Supplementary Figures and Tables

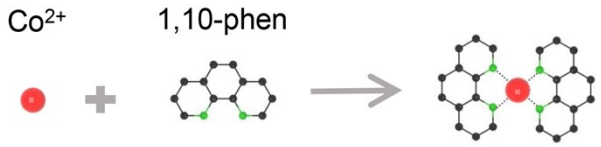

Fig. S1. Schematic of the synthesis of cobalt-1,10-phenanthroline complex.

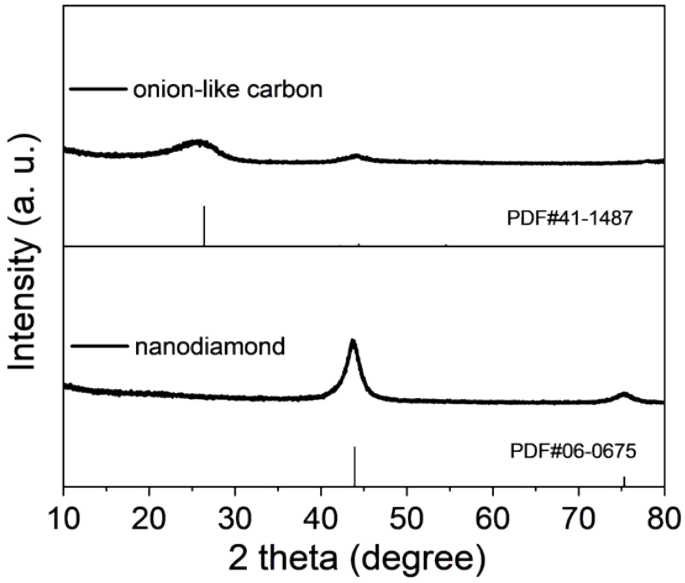

Fig. S2. PXRD patterns of nanodiamond and onion-like carbon.

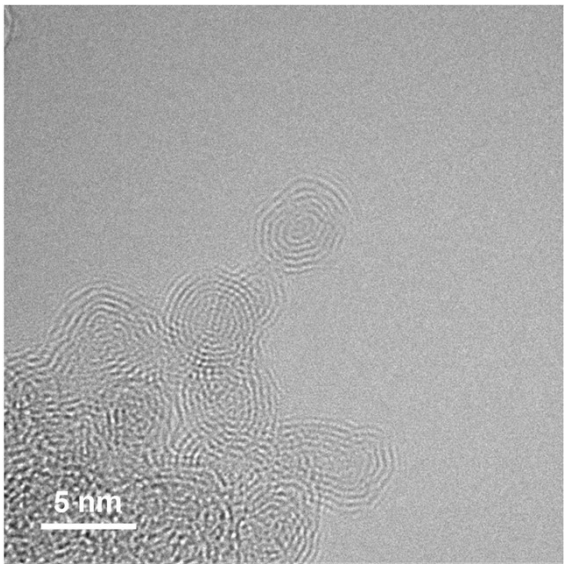

Fig. S3. HRTEM image of the onion-like carbon.

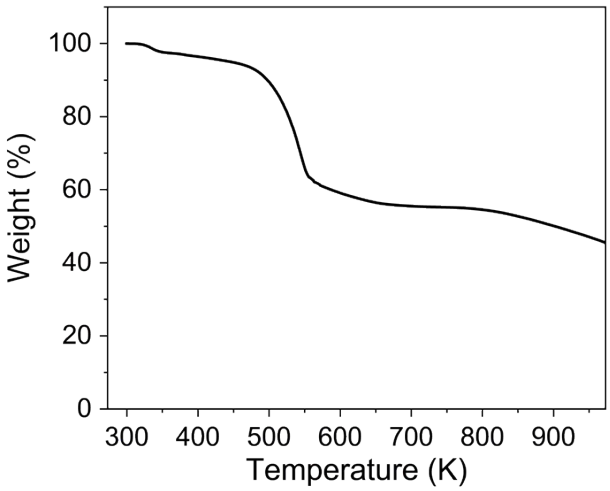

Fig. S4. TGA curve of cobalt-1,10-phenanthroline complex under Ar.

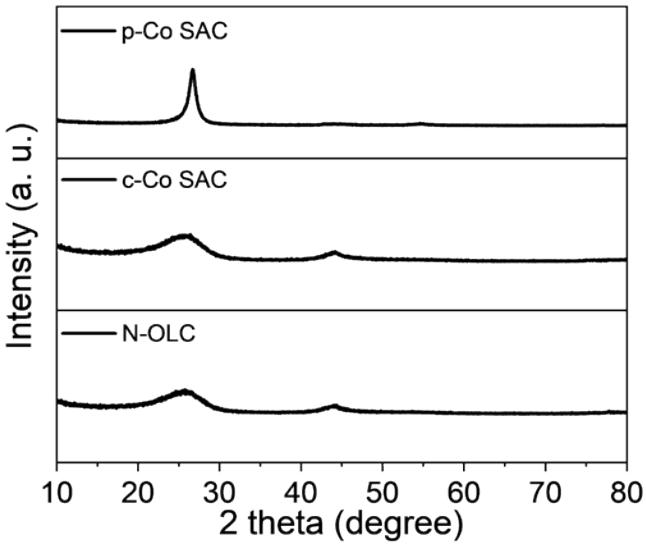

Fig. S5. PXRD patterns of the c-Co SAC, p-Co SAC and N-OLC.

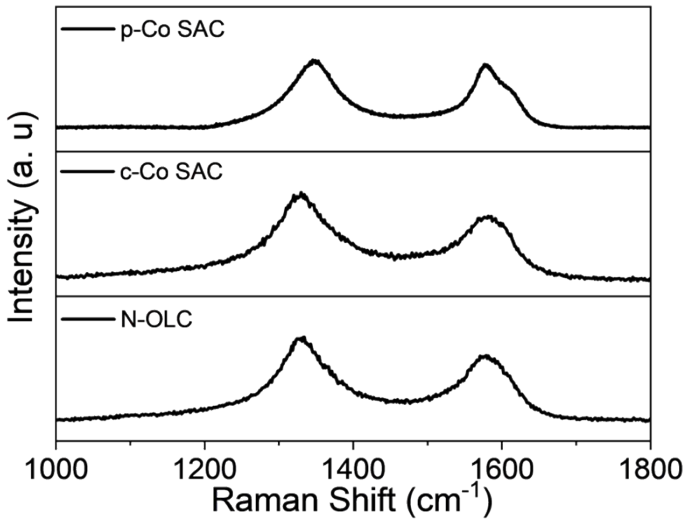

Fig. S6. Raman spectra of the c-Co SAC, p-Co SAC and N-OLC.

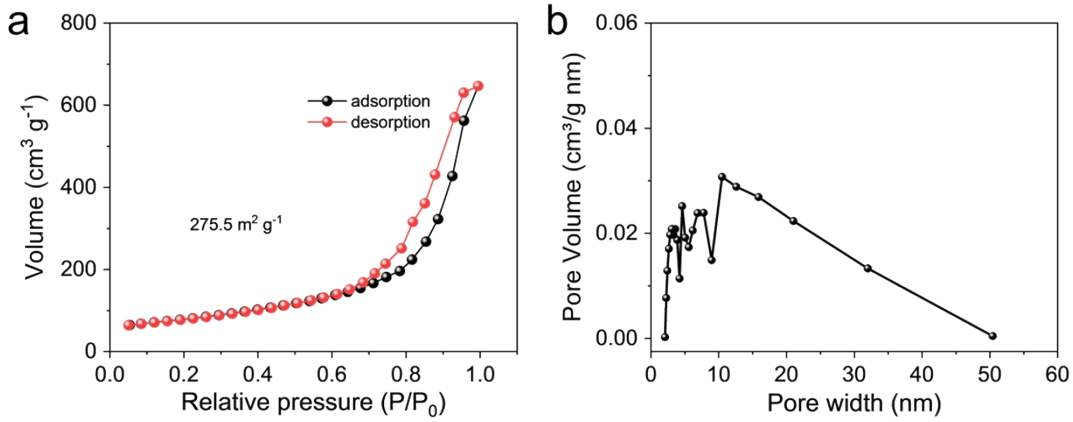

Fig. S7. (a) Nitrogen sorption isotherm, **(b)** pore size distribution of c-Co SAC.

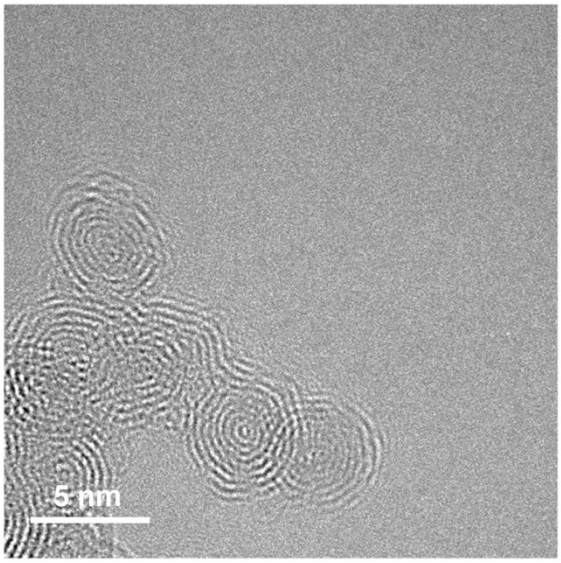

Fig. S8. HRTEM image of the N-OLC.

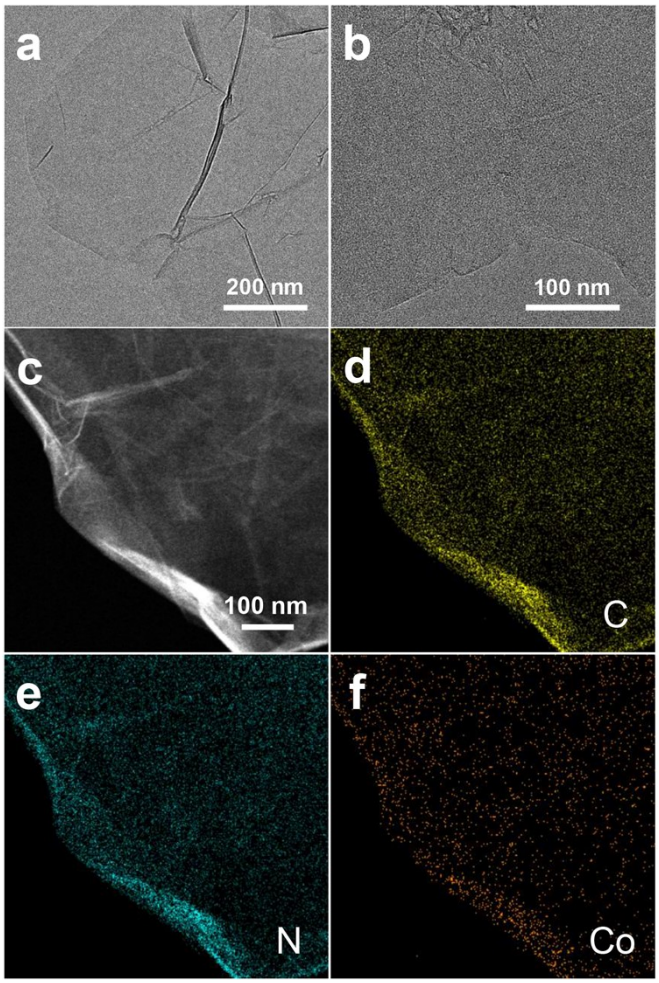

Fig. S9. (a, b) TEM images, **(c-f)** Elemental mapping images of the p-Co SAC.

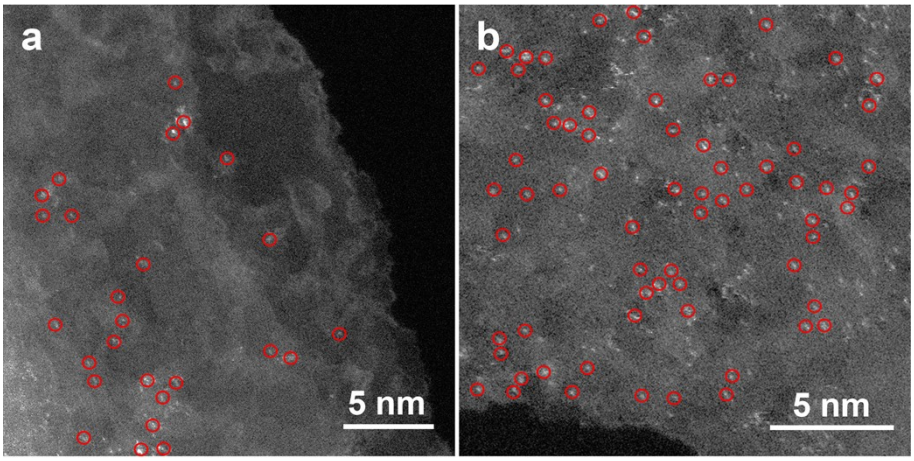

Fig. S10. Aberration-corrected HAADF-STEM images of the p-Co SAC.

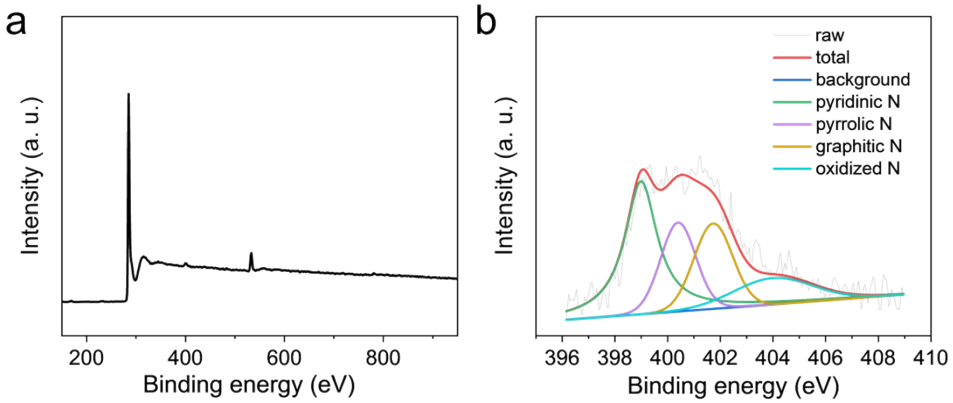

Fig. S11. (a) XPS full survey spectrum, **(b)** N 1s XPS spectrum of c-Co SAC.

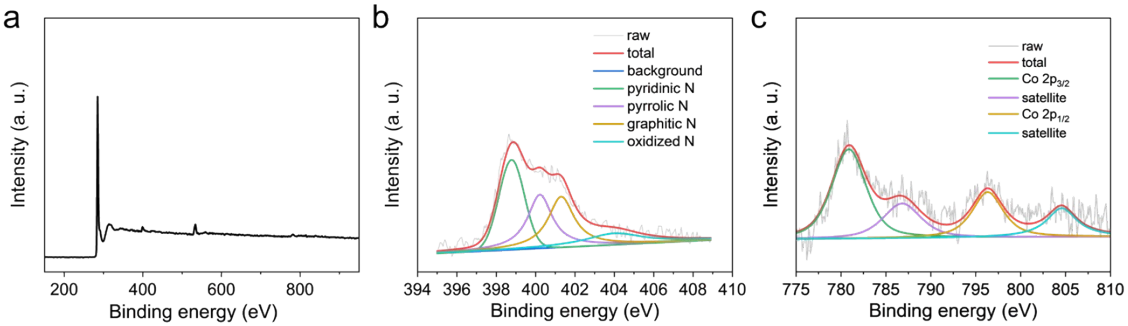

Fig. S12. (a) XPS full survey spectrum, **(b)** N 1s XPS spectrum and **(c)** Co 2p XPS spectrum of p-Co SAC.

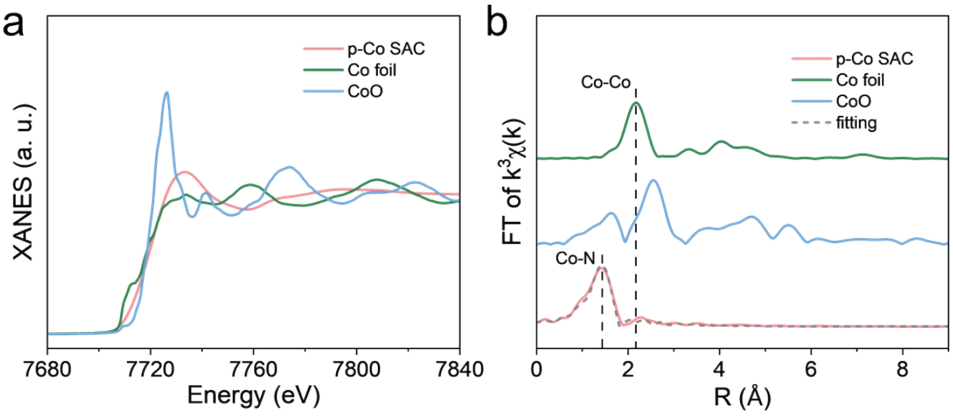

Fig. S13. (a) Co K-edge XANES spectra, **(b)** FT-EXAFS spectra of p-Co SAC, Co foil and CoO.

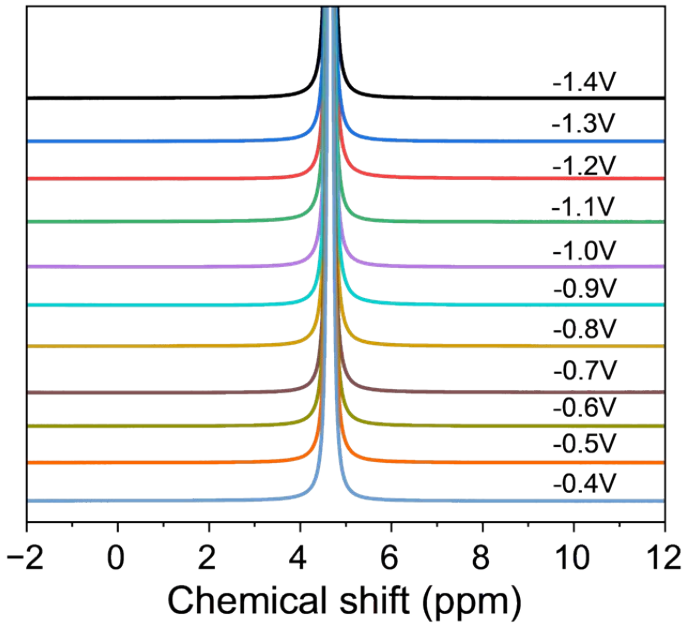

Fig. S14. ^{1}H NMR spectra after CO_2 reduction electrolysis at different potentials using c-Co SAC.

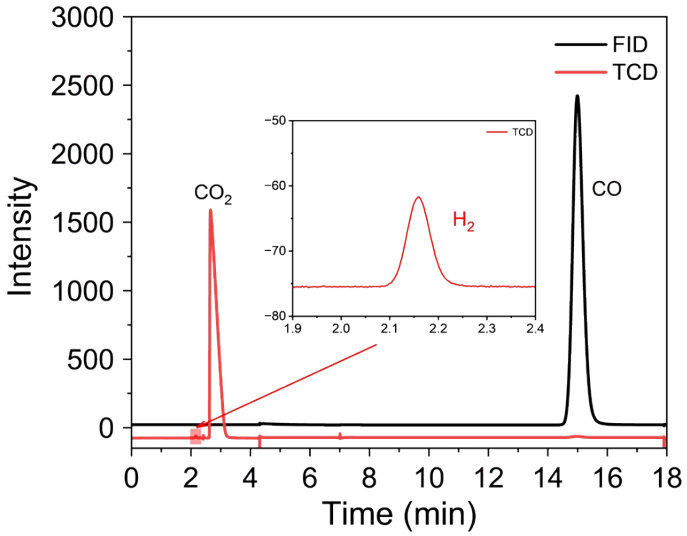

Fig. S15. GC profile during CO_2 reduction electrolysis at -0.8 V *vs*. RHE using c-Co SAC.

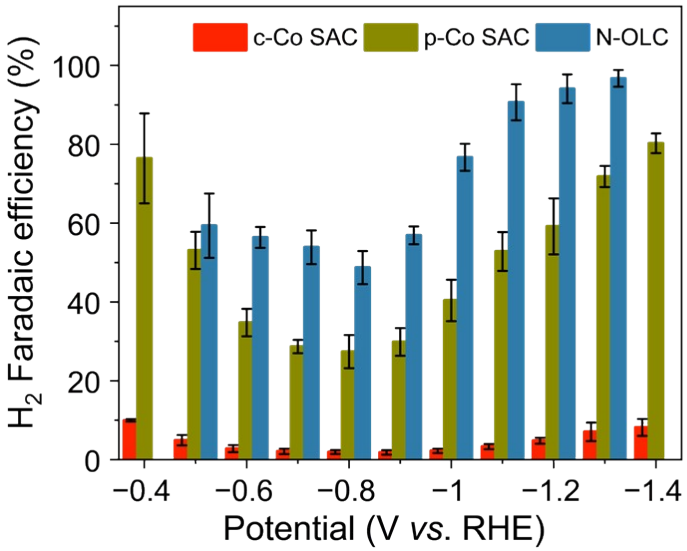

Fig. S16. H_2 Faradaic efficiency of c-Co SAC, p-Co SAC and N-OLC.

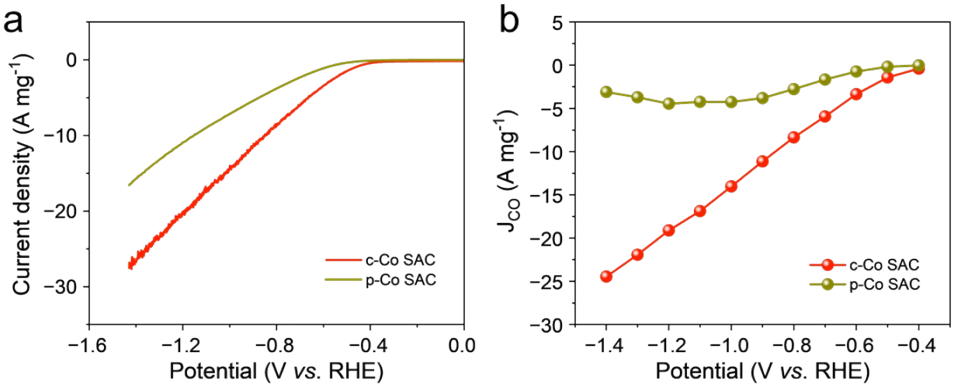

Fig. S17. (a) Total current, **(b)** CO current in H-cell normalized by metal loading.

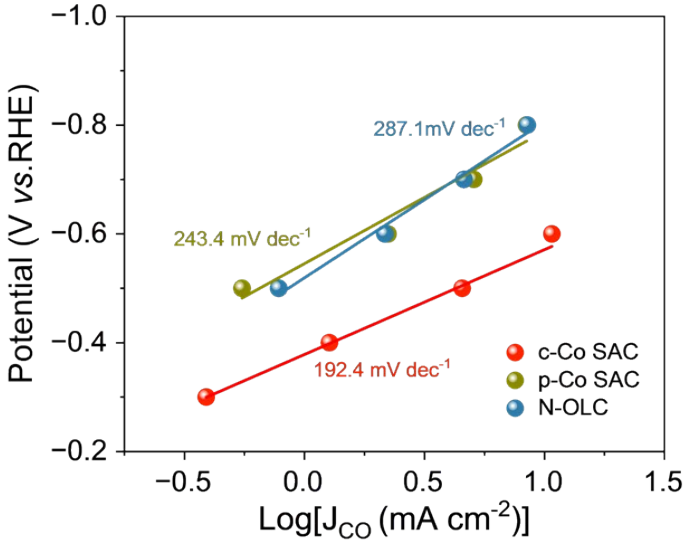

Fig. S18. Tafel slope results of c-Co SAC, p-Co SAC and N-OLC.

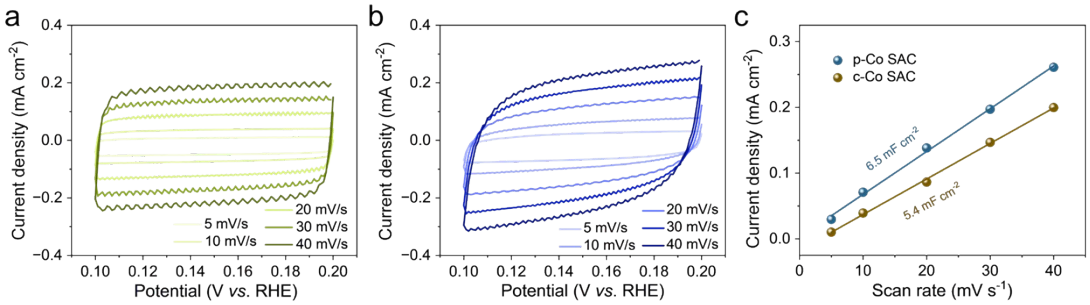

Fig. S19. CV curves of **(a)** c-Co SAC and **(b)** p-Co SAC. **(c)** ECSA results of the catalysts, the current density is taken at 0.18 V *vs.* RHE.

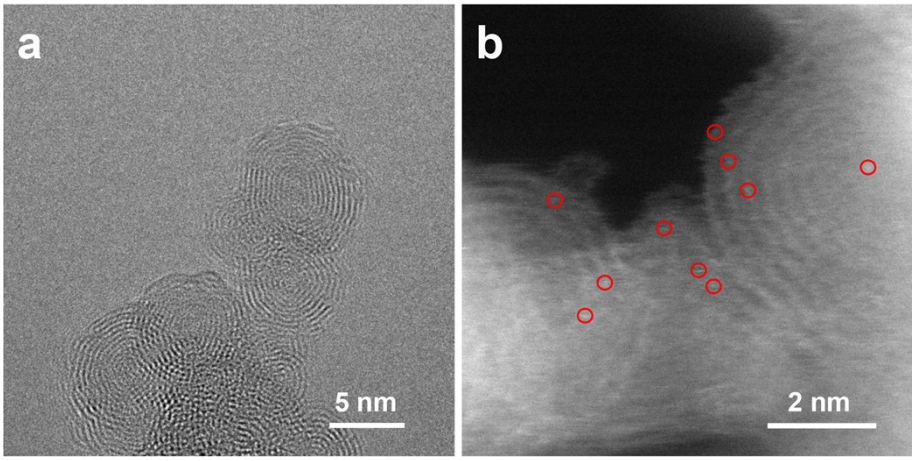

Fig. S20. (a) HRTEM image **(b)** aberration-corrected HAADF-STEM image of the c-Co SAC after stability test.

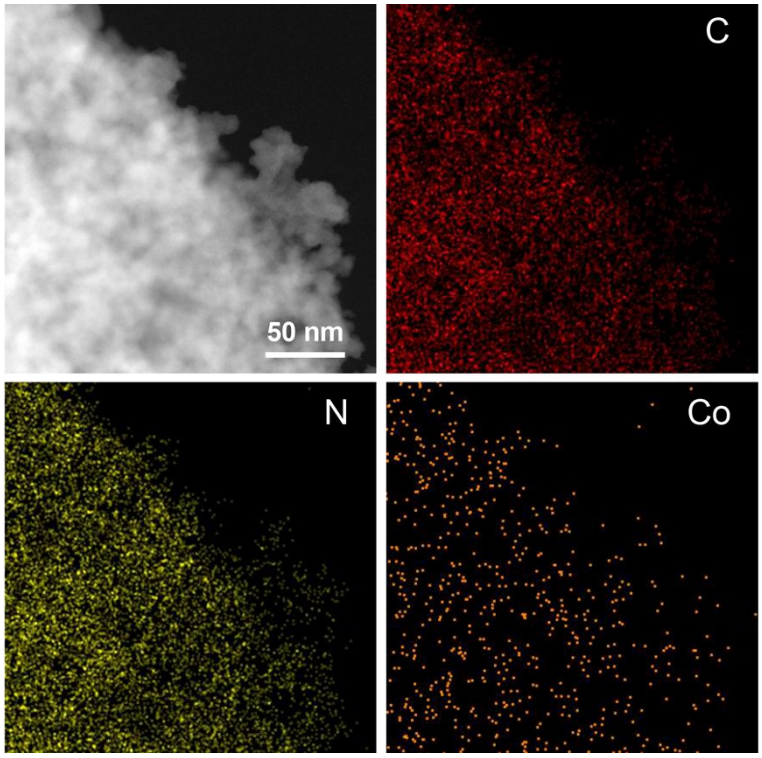

Fig. S21. Elemental mapping images of the c-Co SAC after stability test.

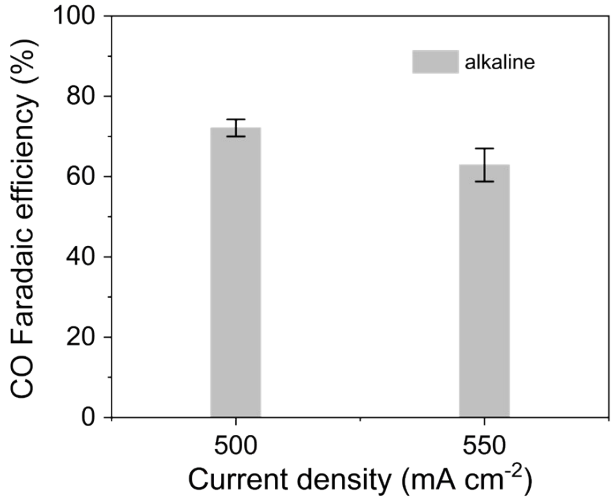

Fig. S22. CO Faradaic efficiency of c-Co SAC in alkaline electrolyte at 500 and 550 mA cm^{-2} current density.

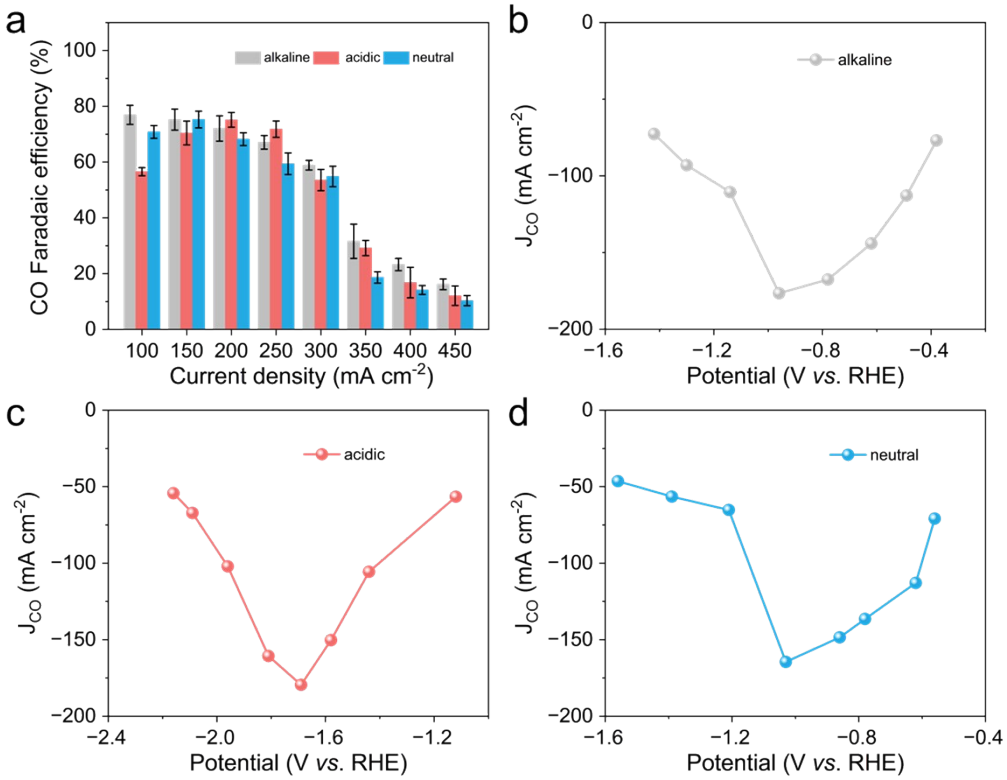

Fig. S23. (a) CO Faradaic efficiency, **(b-d)** CO current density of p-Co SAC in flow cell.

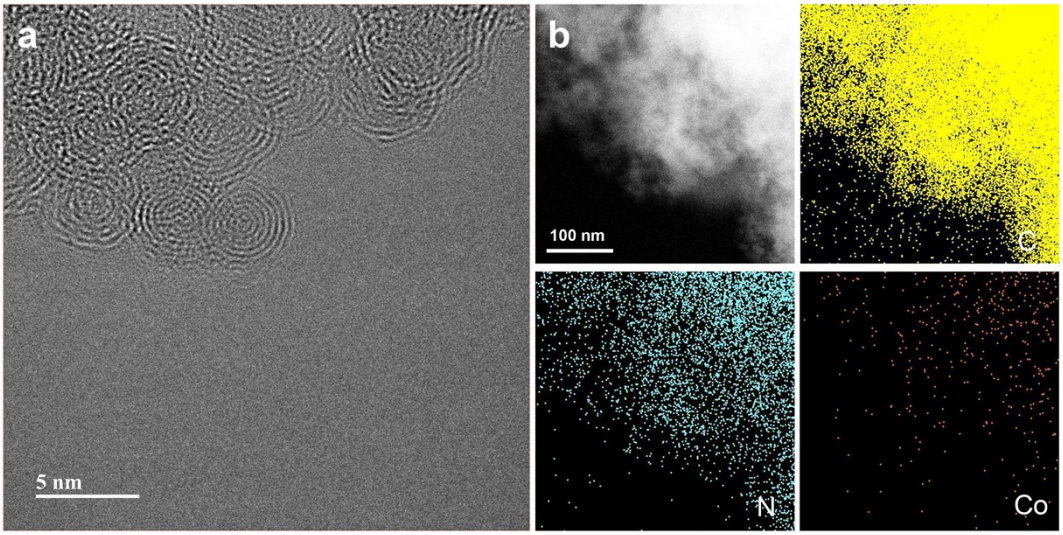

Fig. S24. (a) TEM image, **(b)** elemental mapping of c-Co SAC after stability measurement in flow cell with alkaline electrolyte.

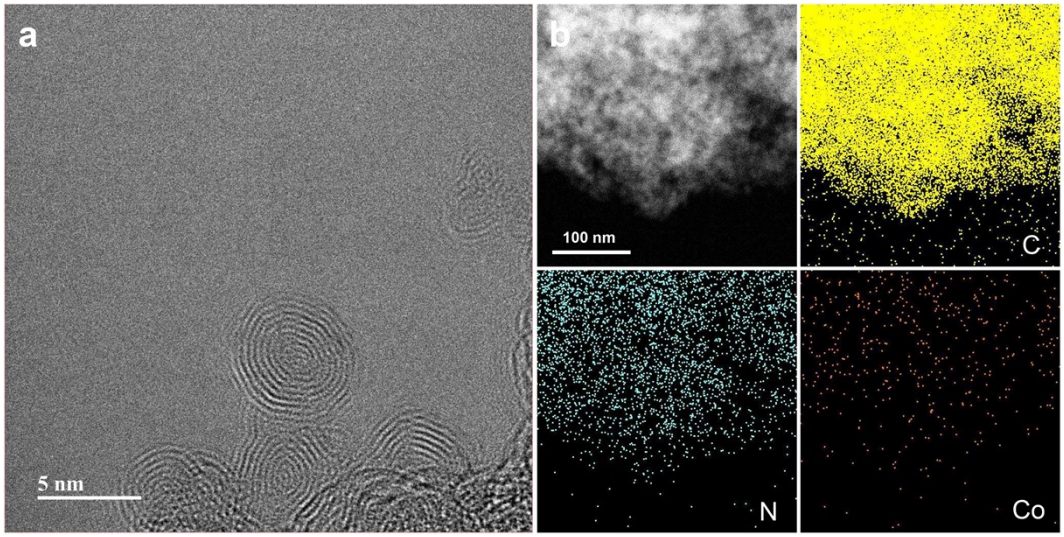

Fig. S25. (a) TEM image, **(b)** elemental mapping of c-Co SAC after stability measurement in flow cell with acidic electrolyte.

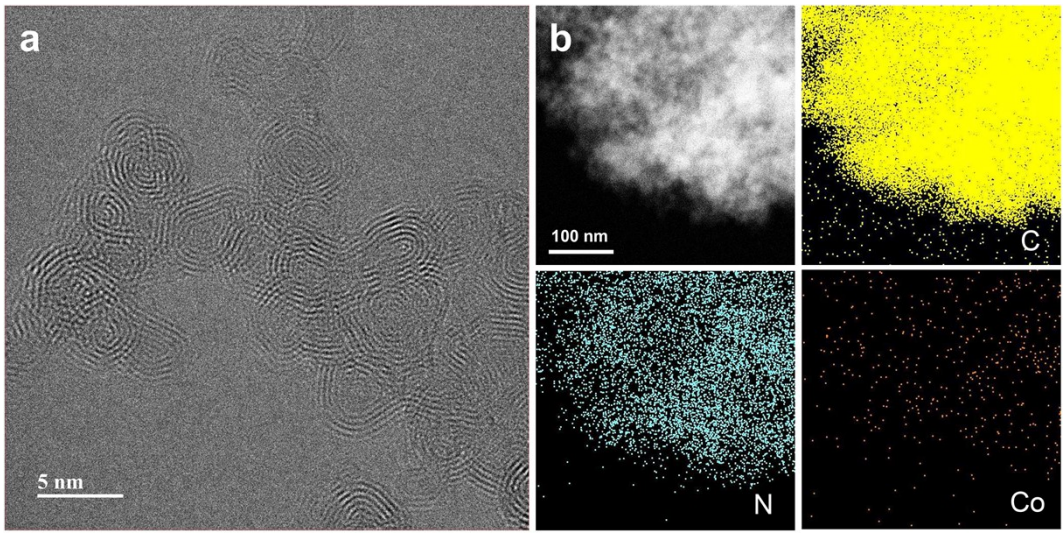

Fig. S26. (a) TEM image, **(b)** elemental mapping of c-Co SAC after stability measurement in flow cell with neutral electrolyte.

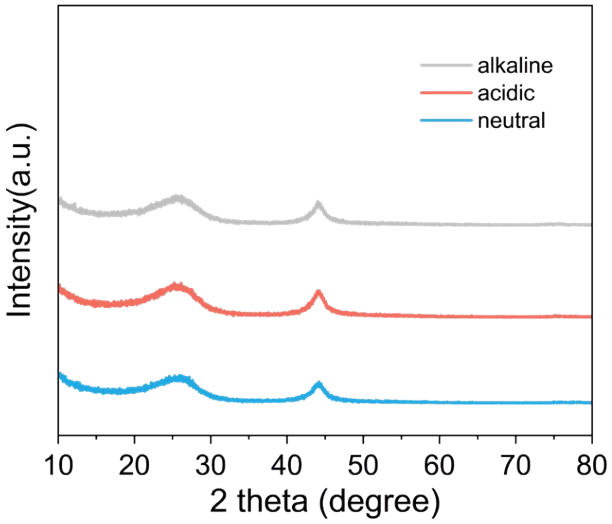

Fig. S27. PXRD patterns of c-Co SAC after stability measurements in flow cell.

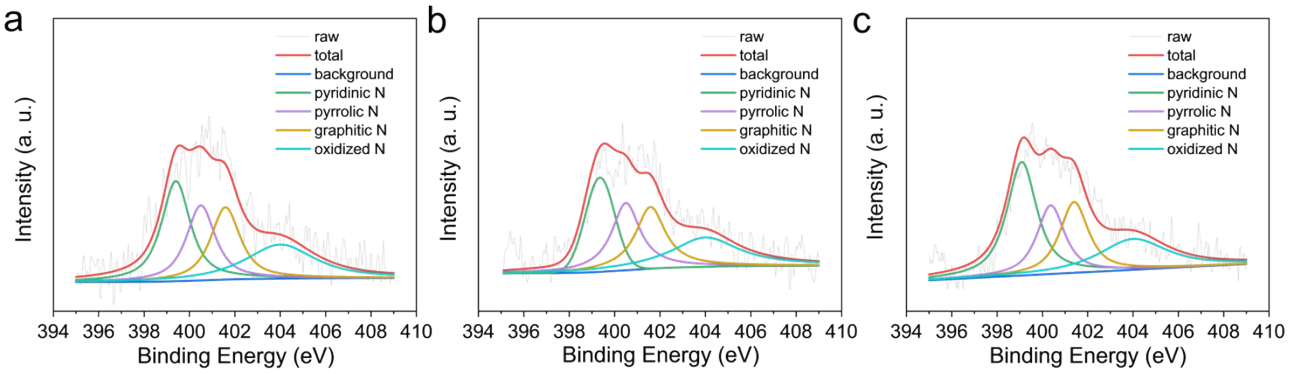

Fig. S28. N 1s XPS spectra of c-Co SAC after stability measurements in flow cell with **(a)** alkaline, **(b)** acidic and **(c)** neutral electrolyte.

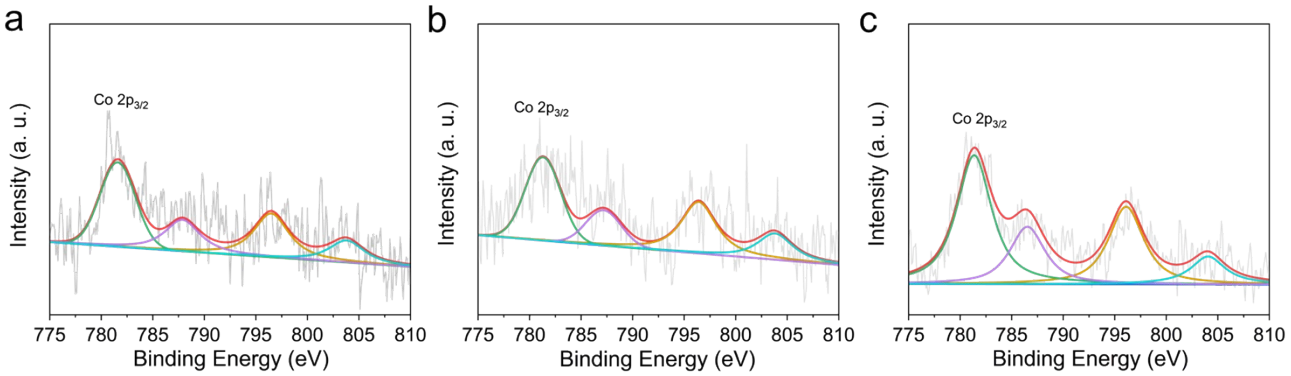

Fig. S29. Co 2p XPS spectra of c-Co SAC after stability measurements in flow cell with **(a)** alkaline, **(b)** acidic and **(c)** neutral electrolyte.

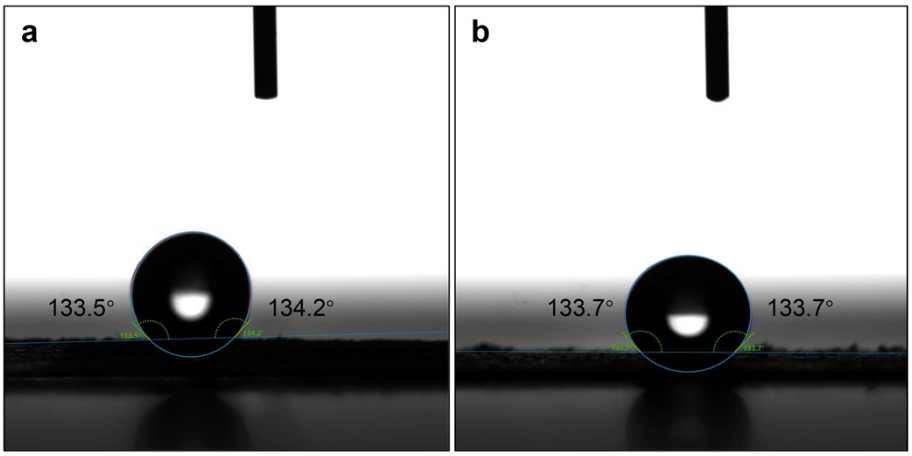

Fig. S30. Contact angle results of (a) c-Co SAC and (b) p-Co SAC.

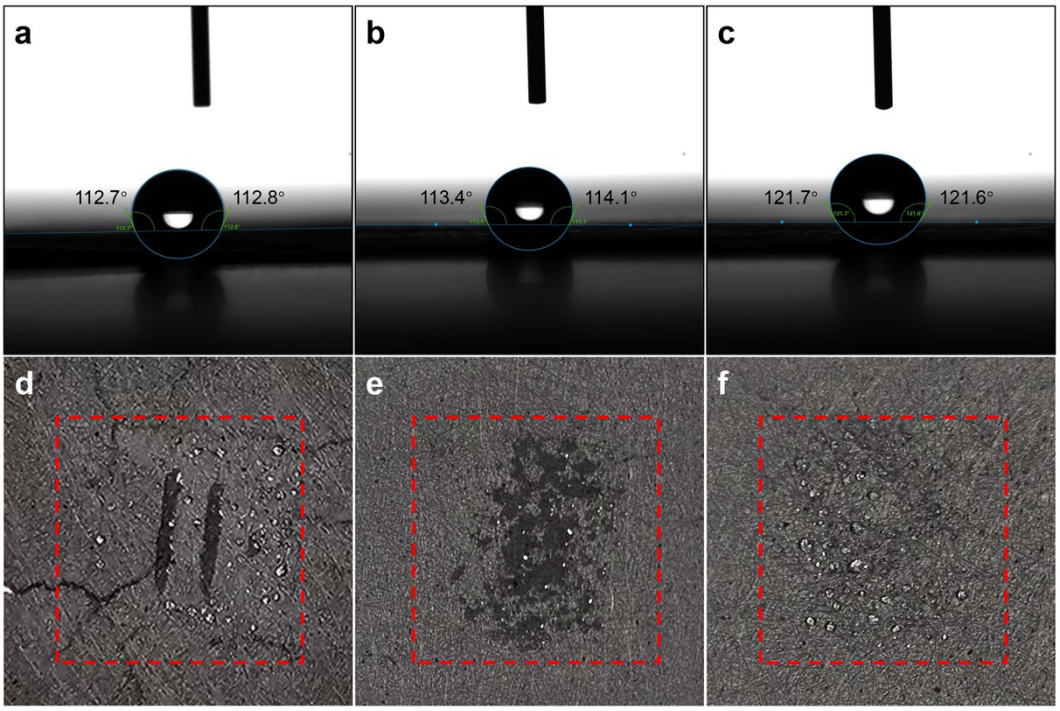

Fig. S31. Contact angle results of c-Co SAC after stability measurements in flow cell with (a) alkaline, (b) acidic and (c) neutral electrolytes. Photographs of the gas-diffusion layer of the cathode after stability measurements in flow cell with (d) alkaline, (e) acidic and (f) neutral electrolytes.

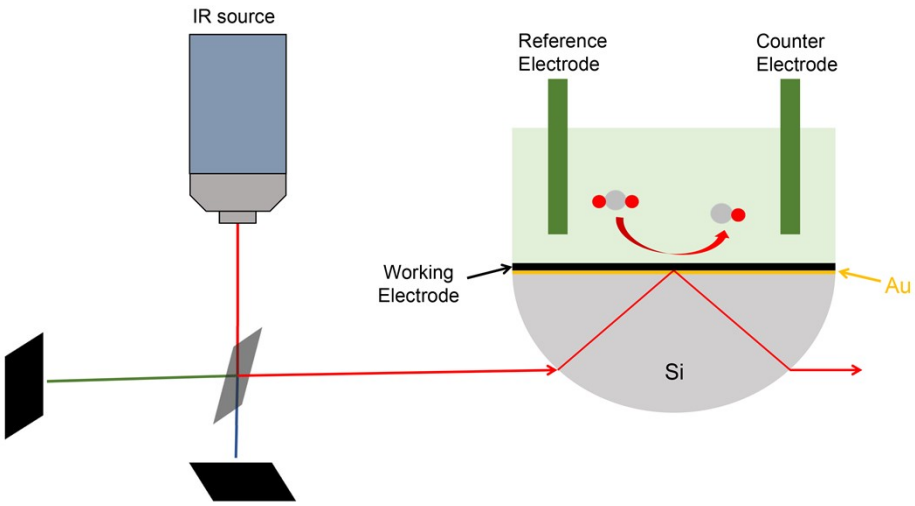

Fig. S32. Schematic of in-situ ATR-IR experiments.

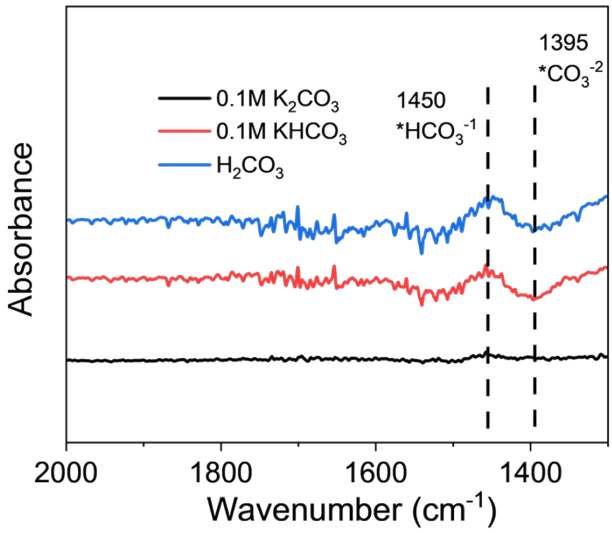

Fig. S33. ATR-IR spectra of different electrolytes.

To verify that peaks at 1450cm^{-1} and 1395cm^{-1} are assigned to HCO_3^- and CO_3^{2-}, We tested the IR signals of 0.1M $KHCO_3$ and H_2CO_3 (CO_2 saturated solution), using 0.1 M K_2CO_3 as a baseline.

The 0.1M $KHCO_3$ solution and H_2CO_3 solution contained more HCO_3^- than the 0.1 M K_2CO_3 solution, so the positive peak at 1450cm^{-1} was assigned to HCO_3^-.

Similarly, the 0.1M $KHCO_3$ solution and H_2CO_3 solution contained less CO_3^{2-} than the 0.1 M K_2CO_3 solution, so the negative peak at 1395 cm^{-1} was assigned to CO_3^{2-}.

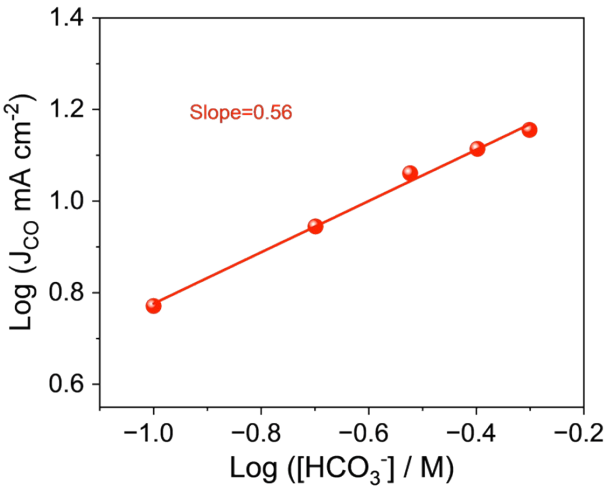

Fig. S34. CO current density versus HCO_3^- concentration plot at -0.8 V *vs.* RHE using c-Co SAC.

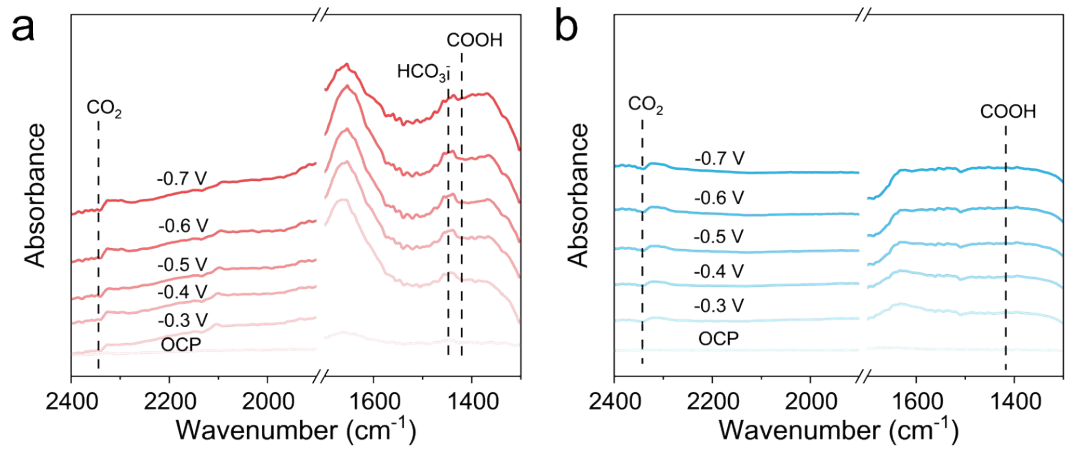

Fig. S35. In-situ ATR-IR spectra of **(a)** c-Co SAC, **(b)** p-Co SAC in 0.05 M H_2SO_4 + 1 M KCl.

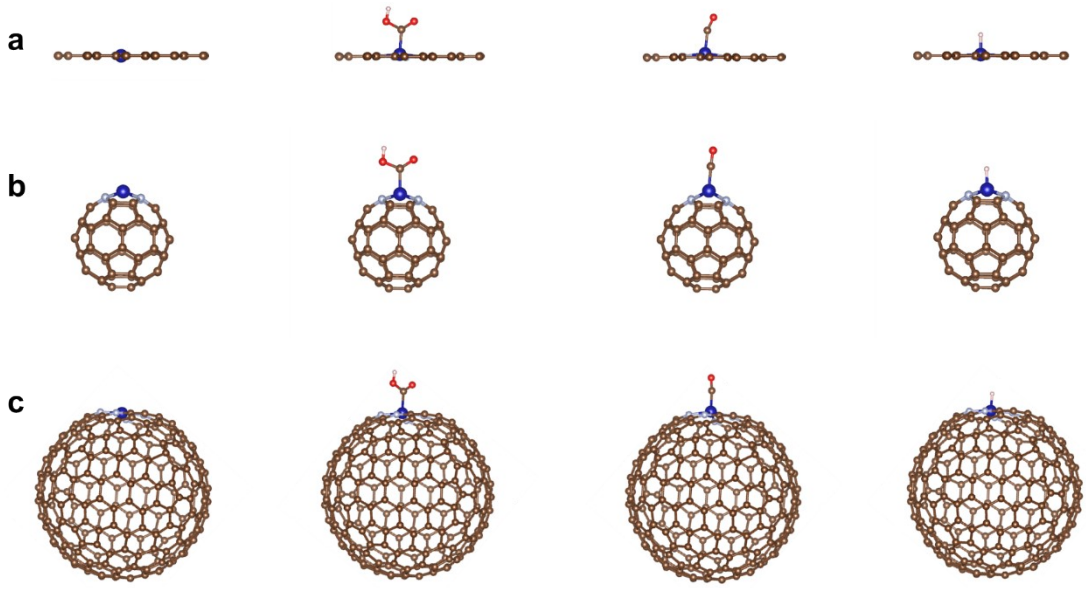

Fig. S36. Optimized structure models of **(a)** Co-N_4-Graphene, **(b)** Co-N_4-C_{60} and **(c)** Co-N_4-C_{240} with *COOH, *CO and *H intermediates.

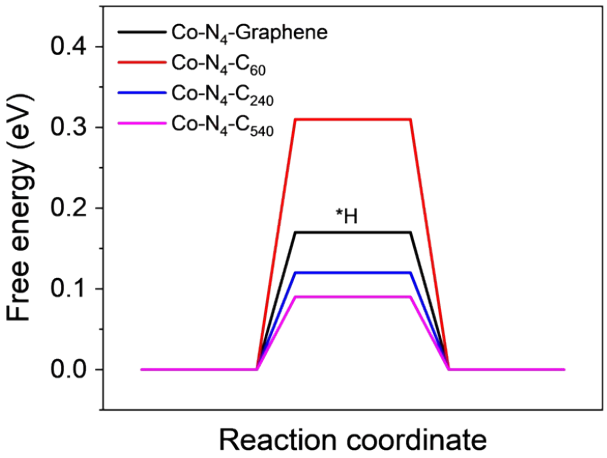

Fig. S37. Free energy diagram of hydrogen evolution reaction on various Co-N_4-C structures.

Table S1. Fit parameters obtained from FT-EXAFS spectra of Co-K edge for the catalysts. C. N. [a]: coordination numbers; R (Å) [b]: bond distance; σ^2 ($\times 10^{-3}$ Å^2) [c]: Debye-Waller factors; ΔE_0 (eV) [d]: the inner potential correction; R factor [e]: goodness of fit.

samples	path	C. N. [a]	R (Å) [b]	σ^2 ($\times 10^{-3}$ Å^2) [c]	ΔE_0 (eV) [d]	R factor [e]
c-Co SAC	Co-N	4.2±1.1	1.94±0.02	7.8±2.7	-7.1±6.1	0.01
p-Co SAC	Co-N	3.8±1.0	1.97±0.02	7.3±3.0	-6.1±3.6	0.01

Table S2. Summary of some recently reported CO_2 electroreduction catalysts in H-type cell.

	Catalyst	Electrolyte	Loading (mg/cm^2)	CO maximum Faradaic efficiency (%)	Potential window CO FE reaches 90% (mV)	TOF (h^{-1})	Reference
1	c-Co SAC	0.5 M $KHCO_3$	0.5	98.2	1000	26725	This Work
2	NiFe-DASC	0.5 M $KHCO_3$	0.4	94.5	400	15055	Nat. Commun. 2021, 12, 4088
3	Ni-Zn-N-C	0.5 M $KHCO_3$	1.0	99	500	~1400	Adv. Mater. 2021, 33, e2102212
4	Fe–N_4-C	0.1 M $KHCO_3$	1.0	90	100	\	Adv. Mater. 2021, 33, 2003238
5	Ni-CNC	0.5 M $KHCO_3$	0.5	96.6	400	\	Angew. Chem. Int. Ed. 2022, 61, e202113918
6	Fe−N/P−C	0.5 M $KHCO_3$	0.75	98	300	508.8	Nano Lett. 2022, 22, 1557
7	NiNG-S	0.5 M $KHCO_3$	1.0	97	300	3965	Angew. Chem. Int. Ed. 2021, 60, 23342
8	NiSA/PCFM	0.5 M $KHCO_3$	1.0	95	500	\	Nat. Commun. 2020, 11, 593
9	H_2-FeN_4/C	0.1 M $NaHCO_3$	0.51	97	500	4900	Chem. 2021, 7, 1297
10	$Zn^{\delta+}$-NC	0.5 M $KHCO_3$	0.25	99	250	~850	Angew. Chem. Int. Ed. 2021, 60, 22826
11	Ni@NiN_4CM	0.5 M $KHCO_3$	1.0	97.6	400	\	Angew. Chem. 2021, 133, 12066
12	InNi DS/NC	0.5 M $KHCO_3$	0.8 ± 0.1	96.7	300	7353	Angew. Chem. Int. Ed. 2023, 62, e202216326
13	Co-CNTs-MW	0.5 M $KHCO_3$	1.0	93.6	400	25896	Nat. Commun. 2023, 14, 1599

Table S3. Summary of some recently reported CO_2 electroreduction catalysts in flow cell with alkaline electrolyte.

	Catalyst	CO maximum Faradaic efficiency (%)	Maximum J_{CO} (mA/cm^2)	Stability	Reference
1	c-Co SAC	98.9	437	10 hours, J: 100 mA/cm^2 FE_{CO}: from 98 % to 97 %	This Work
2	A-Ni@CMK	95	366	5 hours, J: from ~ 135 mA/cm^2 to ~ 125 mA/cm^2 FE_{CO}: from ~ 98 % to ~ 98 %	Adv. Energy Mater. 2021,11, 2102152
3	CdS NNs	95.5	~320	\	Angew. Chem. Int. Ed. 2020, 59, 8706
4	ZrO_2@Ni-NC	96.8	193.5	0.5 hours, J: from ~ 250 mA/cm^2 to ~ 230 mA/cm^2	Adv. Funct. Mater. 2021, 31, 2104243
5	NiSA/PCFM	88	308.4	120 hours J: from ~ 310 mA/cm^2 to ~ 300 mA/cm^2 FE_{CO}: from ~ 92 % to ~ 90 %	Nat. Commun. 2020, 11, 593
6	Cu/Ni-NC	99	489	\	Adv. Mater. 2023, 35, 2209590
7	CoPc/CNT-MT	99	194	\	Adv. Funct. Mater. 2022, 32, 2107301
8	Ni_2-N_4-C_2	97.8	124.5	30 hours, J: from ~ 115 mA/cm^2 to ~ 100 mA/cm^2 FE_{CO}: from 86.3 % to 76.7 %	Angew. Chem. Int. Ed. 2022, 61, e202113918
9	Ni-N_4/C-NH_2	89	450	6 hours, J: from ~ 540 mA/cm^2 to ~ 520 mA/cm^2 FE_{CO}: from ~ 88 % to ~ 82 %	Energy Environ. Sci., 2021, 14, 2349
10	CoPc2	96	165	3 hours, J: from ~ 115 mA/cm^2 to ~ 110 mA/cm^2	Nat. Commun. 2019, 10, 3602
11	CoTMAPc @CNT	95.6	239	15 hours, J: from ~ 30 mA/cm^2 to ~ 27 mA/cm^2 FE_{CO}: from ~ 94 % to ~ 92 %	Energy Environ. Sci. 2021, 14, 483
12	CoPc-carbon	95	~160	20 hours, J: from ~ 55 mA/cm^2 to ~ 50 mA/cm^2 FE_{CO}: from ~ 87 % to ~ 72 %	Science 2019, 365, 367
13	Ag coral	90	312	30 hours, J: 100 mA/cm^2 FE_{CO}: from ~ 98 % to ~ 98 %	Nano Energy 2020, 76, 105030
14	Au/C	\	\	10 hours, J: 100 mA/cm^2 FE_{CO}: from ~ 93 % to ~ 85 %	Nat. Commun. 2020, 11, 3028
15	Fe porphyrin	98.8	152	24 hours, J: from ~ 30 mA/cm^2 to ~ 25 mA/cm^2 FE_{CO}: from ~ 98.5 % to ~ 98 %	Chem. Eur. J. 2020, 26, 3034
16	Ag–S–C3N4/CNT	93	186	4 hours J: from ~ 260 mA/cm^2 to 250 mA/cm^2 FE_{CO}: from ~ 95 % to ~ 85 %	Mater. Today Phys. 2020, 12, 100176

Table S4. Summary of some recently reported CO_2 electroreduction catalysts in flow cell with acidic electrolyte.

	Catalyst	Electrolyte	CO maximum Faradaic efficiency (%)	Maximum J_{CO} (mA/cm^2)	Stability	Reference
1	c-Co SAC	0.05 M H_2SO_4+1 M KCl	96.5	337	10 hours, J: 100 mA/cm^2 FE_{CO}: from 85 % to 80 %	This Work
2	Ni-N-C 60% PTFE	1 M Cs_2SO_4+0.5 M H_2SO_4	99.5	249	36 hours, J: 100 mA/cm^2 FE_{CO}: from ~ 95 % to ~ 90 %	Adv. Mater. 2022, 34, 2201295
3	CuNi-NC	0.1 M H_3PO_4+0.9 M KH_2PO_4+1.1 M KCl	99	190	25 hours, J: 100 mA/cm^2 FE_{CO}: from ~ 98 % to ~ 90 %	Adv. Mater. 2023, 35, 2209590
4	NiPc-OMe MDE	0.5 M K_2SO_4+5 mM H_2SO_4	99	396	12 hours, J: 100 mA/cm^2 FE_{CO}: from ~ 95 % to ~ 90 %	Adv. Energy Mater. 2023, 13, 2203603
5	Au	1 M Cs_2SO_4+0.5 M H_2SO_4	90	180	\	Nat. Commun. 2021, 12, 4943
6	Co:P4VP	0.01 M H_2SO_4+0.1 M Na_2SO_4	92	78.2	\	Adv. Energy Mater. 2020, 10, 2001645
7	Au/C	0.1M H_2SO_4+0.4M K_2SO_4	91	125	4 hours, J: 200 mA/cm^2	Nat. Catal. 2022, 5, 268

Table S5. Summary of some recently reported CO_2 electroreduction catalysts in flow cell with neutral electrolyte.

	Catalyst	Electrolyte	CO maximum Faradaic efficiency (%)	Maximum J_{CO} (mA/cm^2)	Stability	Reference
1	c-Co SAC	1 M $KHCO_3$	98.6	367	10 hours, J: 200 mA/cm^2 FE_{CO}: from 95 % to 89 %	This Work
2	CoPc/GDY/G	1 M $KHCO_3$	97	97	\	J. Am. Chem. Soc. 2021, 143, 8679
3	CA/N-Ni aerogel	1 M $KHCO_3$	91	300	50 min, J: 100 mA/cm^2 FE_{CO}: from ~ 97 % to ~ 91 %	Adv. Funct. Mater. 2021, 31, 2104377
4	Ni_2-N_4-C_2	1 M $KHCO_3$	93	~90	\	Angew. Chem. Int. Ed. 2022, 61, e202113918
5	NiPc–OMe MDE	1 M $KHCO_3$	95	150	40 hours, J: 150 mA/cm^2 FE_{CO}: from ~ 98 % to ~ 90 %	Nat. Energy 2020, 5, 684
6	Ni–N–C	1 M $KHCO_3$	85	225	20 hours, J: 200 mA/cm^2 FE_{CO}: from ~ 81 % to ~ 81 %	Energy Environ. Sci. 2019, 12, 640
7	NiSA/PCFM	0.5 M $KHCO_3$	83	336.5	120 hours, J: form ~ 310 mA/cm^2 to ~ 295 mA/cm^2 FE_{CO}: from ~ 91 % to ~ 90 %	Nat. Commun. 2020, 11, 593
8	CuNi-NC	1 M $KHCO_3$	99	225	\	Adv. Mater. 2023, 35, 2209590